NUMERICAL MODELS FOR PLASMA-SOLID INTERACTIONS IN ELECTROTHERMAL MASS ACCELERATORS

GT - Devices

5705A General Washington Drive Alexandria, VA 22312 (703) 642-6150

2

NUMERICAL MODELS FOR PLASMA-SOLID INTERACTIONS IN ELECTROTHERMAL MASS ACCELERATORS

Niels K. Winsor, Derek A. Tidman and Shyke A. Goldstein

GT-Devices, Inc.
5705 A General Washington Drive
Alexandria, VA 22312

June 1985

Final Report

Of Work Performed For:

Army Research Office
P.O. Box 12211
ATTN: Dr. D. Mann
Research Triangle Park, NC 27709

Contract No. DAAG29-82-C-0013

ARO Project No. P-19060-EG-S

Unclassified

SECURITY CLASSIFICATION OF THIS PAGE (When Data Entered)

REPORT DOCUMENTATION PAGE

READ INSTRUCTIONS BEFORE COMPLETING FORM

1. REPORT NUMBER: ARO 19060.2-EG-S	2. GOVT ACCESSION NO.: AD-A158 637
3. RECIPIENT'S CATALOG NUMBER:	
4. TITLE (and Subtitle): Numerical Models for Plasma-Solid Interactions in Electrothermal Mass Accelerators	5. TYPE OF REPORT & PERIOD COVERED: 22 Jun 82-21 Jun 85 Final Report
	6. PERFORMING ORG. REPORT NUMBER:
7. AUTHOR(s): Niels K. Winsor, Derek A. Tidman, Shyke A. Goldstein	8. CONTRACT OR GRANT NUMBER(s): DAAG29-82-C-0013
9. PERFORMING ORGANIZATION NAME AND ADDRESS: GT-Devices, Alexandria, VA	10. PROGRAM ELEMENT, PROJECT, TASK AREA & WORK UNIT NUMBERS:
11. CONTROLLING OFFICE NAME AND ADDRESS: U. S. Army Research Office, Post Office Box 12211, Research Triangle Park, NC 27709	12. REPORT DATE: Jun 85
	13. NUMBER OF PAGES: 45
14. MONITORING AGENCY NAME & ADDRESS (if different from Controlling Office):	15. SECURITY CLASS. (of this report): Unclassified
	15a. DECLASSIFICATION/DOWNGRADING SCHEDULE:

16. DISTRIBUTION STATEMENT (of this Report)

Approved for public release; distribution unlimited.

17. DISTRIBUTION STATEMENT (of the abstract entered in Block 20, if different from Report)

18. SUPPLEMENTARY NOTES

The view, opinions, and/or findings contained in this report are those of the author(s) and should not be construed as an official Department of the Army position, policy, or decision, unless so designated by other documentation

19. KEY WORDS (Continue on reverse side if necessary and identify by block number)

Electrothermal Mass Accelerators
Accelators
Computer Models
Mass Accelerators

20. ABSTRACT (Continue on reverse side if necessary and identify by block number)

This report describes the physics contents of codes and the results of applying them to simulations of electrothermal mass accelerators. The overall objective ~~of this work~~ was to investigate the dynamics of these accelerators including 2D effects. (over)

DD FORM 1 JAN 73 1473 EDITION OF 1 NOV 65 IS OBSOLETE

A

UNCLASSIFIED

SECURITY CLASSIFICATION OF THIS PAGE (When Data Entered)

20. ABSTRACT CONTINUED:

This has involved the development of computer models for the interactions of multi-species plasma with solid surfaces in single and multiple module plasma mass accelerators. The models are being used to make choices between materials and discharge cavity designs most suitable for achieving long lifetime and high rep-rate performance for these accelerators.

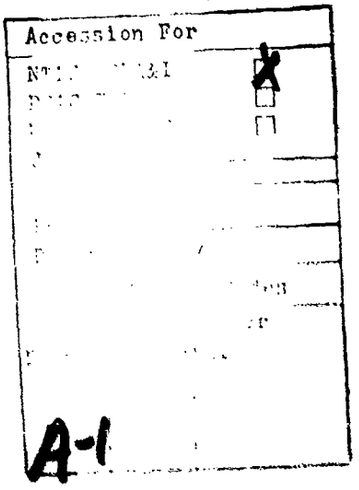

TABLE OF CONTENTS

1. INTRODUCTION

This report describes the physics contents of codes and the results of applying them to simulations of electrothermal mass accelerators. The overall objective of this work is to investigate the dynamics of these accelerators including 2D effects. This has involved the development of computer models for the interactions of multi-species plasma with solid surfaces in single and multiple module plasma mass accelerators. The models are being used to make choices between materials and discharge cavity designs most suitable for achieving long lifetime and high rep-rate performance for these accelerators.

Computer models with axisymmetric 2D elements have been developed for the high density and temperature (1 to about 6 eV) plasmas generated in an electric current driven mass accelerator. The models include a driving circuit for generating the plasma, energy transport models for thermal conduction, radiation transport, and Joule heating, and estimates of shock propagation into low and high-density regions. This model is able to describe the behavior and ablation of plasma in interaction with confining surfaces.

Several computer codes have been developed under this effort. These in turn have benefited from other codes and modules for physics and numerical simulation. Table 1.1 shows many of these codes. This report describes the physics assumptions, geometric models and results obtained during this effort.

Section 2 describes the physical dynamics of the model. It presents both the physics phenomena and the chemistry of the plasma and ablatable wall materials. Section 3 describes the structure of electrothermal systems. It explains the internal geometry of the accelerators. Section 4 presents simulations

Code	Dimensions	Description
MAID 1-7	0	Development versions of cartridge and multi-module simulation code
MAID 8	0	Rewrite of simulation code, incorporating more physics
ABLATE	1	Ablation hydrodynamics code for high resolution of projectile surface
KIWI	0	Multi-Module System Design Code
SESAME	0	Los Alamos Atomic Physics equation-of-state routines
GAPC	1,2	Marder (Los Alamos Lab) hybrid fluid-particle hydrocode
EQMSAP	0	Dielectronic atomic physics equation-of-state and radiaction routines (Princeton University)
FCT	1,2,3	Boris (Naval Research Lab) fluid hydrodynamics code, designed for treatment of shocks
ADINC	1,2	Book (Naval Research Lab) fluid dynamics code for incompressible fluids
PCAP	0	Circuit analysis program (Princeton University)

Table 1.1

which can be compared with experiment. Section 5 presents results and predictions for which experimental data is not yet available. Finally, Section 6 draws conclusions based on the described results.

2. PHYSICS ELEMENTS OF THE MODELS

The basic physics of electrothermal accelerators is very simple in principle. Electric energy is fed into a confined volume. This energy is converted into plasma pressure. The pressure accelerates a projectile down a tube which acts like a gun barrel. In multi-module systems, additional electrical energy conversion modules are arranged along the tube to give additional "kicks" to the projectile.

The physics is considerably more complicated in practice. The plasma is produced by ablation of materials from the interior of the device. The plasma is Joule heated by the electric power input, but various transport processes rapidly redistribute this energy. Finally, the behavior of the plasma atoms and molecules is far from that of an ideal gas or other simple model.

Each of these major physical phenomena affects the dynamics of an electrothermal accelerator. The following subsections describe each of them.

2.1 EXTERNAL DRIVING CIRCUIT

In a convential gun cartridge, a chemical charge supplies the energy propelling the projectile. In an electrothermal accelerator, this energy is supplied by an external electric circuit. In these codes, the energy can be modeled in several ways.

First, a power input can be prescribed. The user can give the power as an experimental or constructed function of time. Alternatively, the electric current can be given and a separate model for the plasma resistance can be used to calculate the voltage and power input.

It is also possible to directly solve a circuit equation. For example, for a simple RLC circuit, the external circuit is described by two equations, one for the current

$$\frac{dI}{dt} = - (IR+Q/C)/L, \tag{2.1}$$

with L and C the lumped circuit inductance and capacitance, and R the dynamic plasma resistance. The second equation is for the charge in the capacitor

$$\frac{dQ}{dt} = I \ . \tag{2.2}$$

These equations are simultaneously solved with the equations for the internal dynamics.

2.2 ABLATION OF SOLIDS

In classical plasma physics, the energy a plasma atom carries is considered "lost" when the atom reaches the wall of the container. This is not the case here. In the normal operation of an electrothermal cartridge, heat is transported to the wall of the cartridge much faster than the wall can transport it away from its surface.

The physical behavior of the cartridge wall during a discharge is analogous to the behavior of porous wood saturated with water, thrown into a fire. The wood doesn't burn, but a lot of steam is produced. The steam is found to carry away most of the energy extracted from the fire.

The "wall" of this discussion includes the physical wall of the cartridge. It also includes the surface of any powder or liquid fill, and the surface of the ablator on the rear of the projectile. This total surface area is subjected to very intense radiation, conduction and other energy transport mechanisms.

If a energy flux, q, is incident on the wall, then an element of surface area, dA, ablates mass at a rate

$$\frac{dm}{dt}\, dA = \frac{q\, dA}{H_s(T)} \tag{2.3}$$

where $H_s(T)$ is the specific enthalpy ($H_s \equiv H/\rho = (W+P)/\rho$, in Joules per kilogram) of the wall material at the plasma temperature, T. This mass enters the bulk plasma with the local specific enthalpy, so it contributes to the local mass density, but not to the momentum or energy density. All equations in this report use MKSI units for all variables except the temperature, which is expressed in electron volts (1 eV = 11,602°K).

Suppose the volume, V, occupied by the ablated material is known. Then

$$\frac{d\,\ell n(\rho)}{dt} = \frac{q\, dA}{H_s(T)} - \frac{d\,\ell nV}{dt} \tag{2.4}$$

This is the equation for the evolution of the mass density.

2.3 CONFINED PLASMA FLUIDS

In the plasma cartridge, ablated mass rapidly establishes a high-pressure quasi-equilibrium plasma. The external power source supplies the energy, and pressure, $P = \rho R \bar{T}$. The mass ablation rate then determines the balance between ρ and $\bar{T}$ in P.

The pressure, P, is the parameter of primary interest, because it is the driving force behind the projectile. We express it in terms of the internal energy W. The pressure can be

written as

$$P = (\gamma - 1)W \tag{2.5}$$

where W is determined primarily by the external power, and is the adiabatic constant of the gas if it behaves like an ideal gas. For our purposes, γ is defined by Eq. 2.5 through the equation of state of the plasma.

2.4 JOULE HEATING

The external energy supply delivers power to the plasma through Joule heating. The power density, p, deposited in the plasma is determined by Ohm's Law

$$p_{OH} = \eta j^2 \tag{2.6}$$

with the resistivity, η, determined by the plasma properties. The resistivity is related to the resistance, R, by the geometry. For a cylinder of length L_c and radius r_c, the resistance is

$$R = \frac{L_c}{r_c^2}\,\eta = 1.7 \times 10^{-5}\,\frac{L_c\, Z\, \varepsilon n\Lambda}{r_c^2\, T^{3/2}}\left(1 + 2\,\frac{\nu_{eo}}{\nu_{ei}}\right) \text{ ohms}, \tag{2.7}$$

where Z is the mean square average charge state of the plasma ions, $\varepsilon n\Lambda$ is the Debye shielding factor for plasma electrons, and ν_{eo} and ν_{ei} are the electron collision frequencies with respect to neutrals and ions, as defined by

$$\nu_{eo} = n_o\, v_e\, \sigma_{eo} \tag{2.8}$$

and

$$\nu_{ei} = 2.86 \times 10^{-12}\, n_i\, Z^2\, \varepsilon n\Lambda / T^{3/2} \quad . \tag{2.9}$$

where n_0 and n_i are the neutral and ion number densities, v_e is the electron thermal velocity and σ_{eo} is the electron-neutral collision frequency. A practical capillary should have a resistance of 100 mOhms or more, in order to efficiently absorb power from conventional switched power supplies.

2.5 THERMAL TRANSPORT

The high energy densities present in this plasma are transported in a number of ways. Conduction and turbulent convection are particularly complicated. A separate technical report (TN GTD 85-4) discusses them. Radiation is the dominant process in the cartridge.

2.6 RADIATION TRANSPORT

Throughout the evolution of this model, we have tried several different radiation models. Simplest is black body:

$$q_{bb} = \sigma_{bb} T^4 \qquad (2.10)$$
$$= 1.03 \times 10^9 T^4$$

Here the radiation flux per unit surface area depends only on the plasma temperature. However, black body radiation can be produced only if the number density of the radiating atoms is high enough to supply that flux. Among the source mechanisms, the simplest is bremsstrahlung,

$$q_{br} = \sigma_{br} n_e n_i Z^2 T^{\frac{1}{2}} \ell_{br} \qquad (2.11)$$

which is the radiation produced by bare ions interacting with free electrons. Here ℓ_{br} is the length resulting from

integrating the flux at a given point over the radiating volume. When the ion has some bound electrons present, it can also produce line radiation, which can be up to an order of magnitude more intense than bremsstrahlung, at similar temperatures and densities. Note that the radiation flux per unit surface area depends on the number of radiating atoms, and not just the temperature. Finally, when the source and black body radiation rates are comparable, the actual radiation process resembles heat diffusion:

$$q_{rd} = \frac{16}{3} \frac{\ell_{rd}\, q_{bb}}{T} \nabla T \quad , \tag{2.12}$$

where the radiation diffusion mean-free-path assuming inverse bremsstrahlung is a tabulated function of density and temperature. The actual radiation which one would expect is the smallest of these:

$$q_{rad} = \min(q_{bb}, q_{br}, q_{rd}) \quad . \tag{2.13}$$

This is the model we have used for many calculations. This radiation model can be made still more complete by incorporating line radiation, but for the parameter ranges used to date, black body emission is the dominant process.

During the initial breakdown of the plasma, bremsstrahlung and line emission are the dominant radiation processes. Within a few microseconds, for the energy densities we are now producing, the radiation switches to black body. In order to reduce the cost of the numerical simulations, we performed calculations in which we used the full model described above, and compared the results with those from a model using only black body radiation. In a series of benchmark comparisons using both cartridge and multiple-module cases, we found only one case in which the performance of the projectile was significantly altered by using the

simpler model, and then only a 5% change in velocity was observed. Thus we conclude that black body radiation is a satisfactory model for the radiation processes in the device.

2.7 MATERIAL EQUATION OF STATE

The computer models have three equations of state available. One is ideal gas, $P = \rho R T$. The second is a Saha equilibrium model which determines the excited state populations and averages over the state populations to determine the fluid variables. This is computationally expensive. The third, and most frequently used equation of state is a tabular data base for about 150 materials. It is the "Sesame" package from Los Almos Scientific Laboratory.

The Sesame equation-of-state package describes the relations among mass density, specific energy density, pressure and temperature. As it is used in the Maid modules, the mass density ρ(kilograms per cubic meter) and specific internal energy W_S (Joules per kilogram) are the independent variables, and the pressure P (pascals) and temperaure T_K (^{0}K) are determined from them via tables. A number of dependent variables are then derived from these basic quantities.

3. GEOMETRICAL ELEMENTS OF THE MODELS

The electrothermal (ET) accelerator is a device which transforms electrical energy into projectile kinetic energy, using wall-confined plasma flows as an intermediary. The efficiency of this energy conversion process depends on the details of the plasma flow. In the previous section, we examined the physics of the plasma. In this section, we examine the geometry of the channels in which that flow takes place.

3.1 PLASMA DISCHARGE CAPILLARY

The source of plasma material is in a confined volume, usually a narrow cylinder. Figure 3.1 illustrates the major features of such a capillary.

Energy is delivered to the capillary electrically. Energy leaves it in the form of a plasma jet. In a well-designed ET capillary, these two energies are nearly equal, the difference being the energy absorbed in the wall and not returned with ablated material.

The equations of motion for the plasma in the capillary are simply mass, momentum and energy conservation in one dimension,

$$\frac{\partial \rho}{\partial t} + \frac{\partial}{\partial x}(\rho v) = \dot{\rho}_a \quad , \tag{3.1}$$

$$\frac{\partial v}{\partial t} + v\frac{\partial v}{\partial x} + \frac{1}{\rho}\frac{\partial P}{\partial x} = 0 \quad , \tag{3.2}$$

$$\frac{\partial}{\partial t}\left(\tfrac{1}{2}\rho v^2 + W\right) + \frac{\partial}{\partial x}\left[\left(\tfrac{1}{2}\rho v^2 + W + P\right) V\right] = P_{OH} \, . \tag{3.3}$$

Here v is the flow velocity, W is the thermodynamic internal energy and P_{OH} is given by Eq. (2.6).

The solution of these equations in the capillary yields the fluxes in the plasma jet. As shown in Figure 3.2, this plasma jet exits the capillary, typically through a nozzle, into a tube occupied by the projectile.

When the pressures on both sides of the nozzle region are comparable, the flow through it is subsonic, and the nozzle is

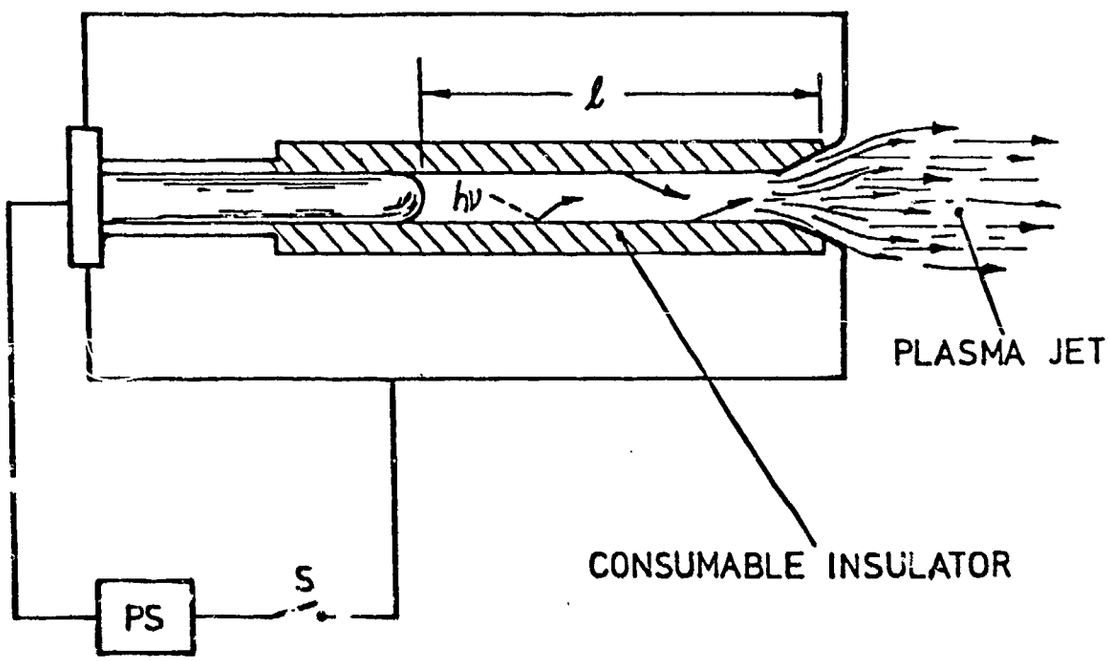

CONSUMABLE WALL CAPILLARY PLASMA JET

Figure 3.1

Ohmic dissipation in the capillary discharge transfers from the electrical store (PS) into the plasma with an efficiency approaching 100%. The discharge functions as a simple resistor in the circuit. This energy is then partitioned between plasma pressure, dissociation, ionization energy, and streaming kinetic energy as plasma is ejected through the nozzle. Energy transport to the wall, principally by radiation, simultaneously ablates its surface, thereby providing additional plasma to maintain the discharge.

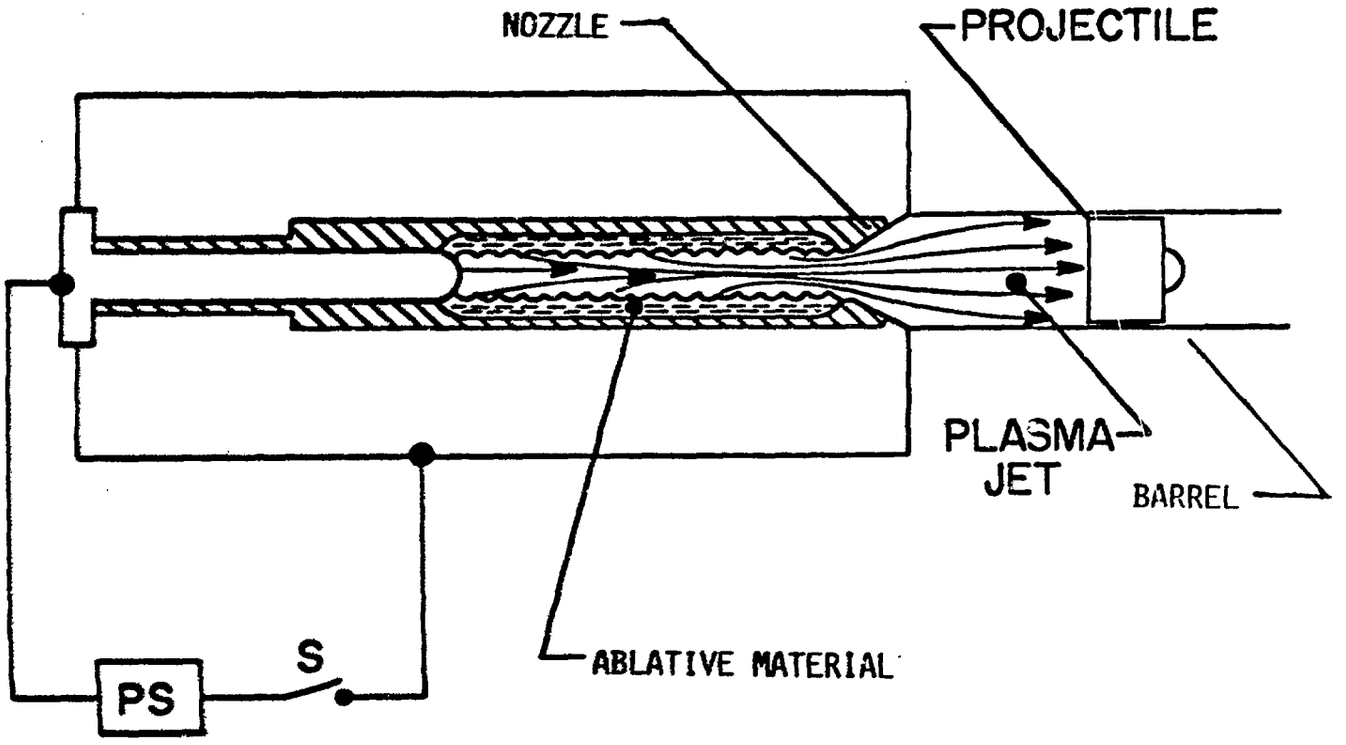

Figure 3.2

An ablative capillary discharge arranged as a cartridge in an electrothermal gun.

ineffective. However, when the projectile is moving rapidly and the capillary pressure, P_c, is much larger than the barrel pressure, P_b, then the nozzle becomes effective. For an ideal gas, it accelerates the flow speed beyond the (critical) sound speed, C_c, in the capillary by a factor

$$M \equiv \frac{v_b}{C_c} = \left(\frac{P_c}{P_b}\right)^{\frac{1}{\gamma}} \frac{A_c}{A_b} \quad , \tag{3.4}$$

where A_c and A_b are the capillary and barrel cross-sectional areas, respectively. The nozzle reduces the temperature by a factor

$$\frac{T_b}{T_c} = \left(\frac{P_b}{P_c}\right)^{\left(\frac{\gamma-1}{\gamma}\right)} \tag{3.5}$$

This lowered temperature in the barrel is very important, because it reduces the heating and ablation of the barrel.

3.2 GUN GEOMETRY

The simplest arrangement of a plasma capillary discharge in a gun geometry is shown in Figure 3.2. It has the virtue of simplicity. It has the disadvantage that it directs hot plasma onto the metal wall of the barrel, ablating the barrel and thus slowing the speed of the plasma jet by adding high-mass metal atoms to the plasma.

Figure 3.3 shows an alternative which improves the flow, but adds to the complexity of the geometry. Figure 3.3A shows the gun before firing. The capillary and projectile are separated by a chamber containing a fluid, such as water, which is readily evaporated by the capillary jet.

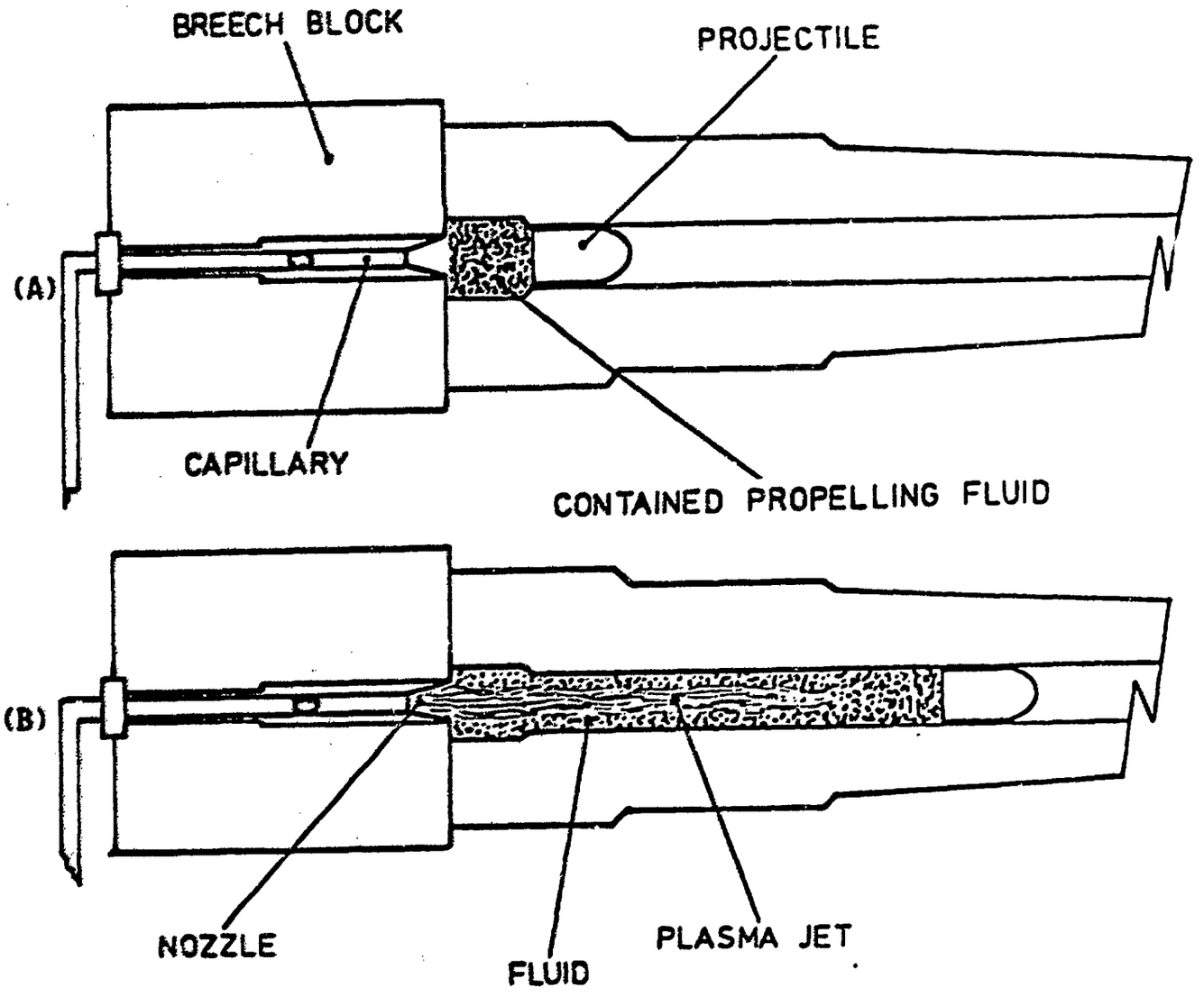

Figure 3.3

A capillary plasma jet may be used as a cartridge in a gun of conventional design. The contained propelling fluid mediates the action of the plasma jet on the gun barrel wall.

Figure 3.3B shows the configuration while the electric discharge is in progress. The hot plasma jet evaporates the propelling fluid, cooling the mixture and protecting the barrel wall from the jet.

The net effect of going to this more complicated geometry is the production of a cooler, denser flow down the gun barrel. That flow then exerts a force on the projectile accelerating down the barrel. The magnitude of that force is less than the pressure at the chamber end of barrel, by a factor,

$$\frac{P_p}{P_b} = \left[1 - \frac{(\gamma-1)U}{2\,C_c}\right]^{\left(\frac{2\gamma}{\gamma-1}\right)} , \qquad (3.6)$$

in conventional guns, where U is the projectile speed. In practice this equation limits the projectile speed to a few times the sound speed for light projectiles, and about 1.2 C_c for heavy projectiles. Turbulent flow also limits the acceleration length of the barrel to 20-100 barrel diameters, as described in an accompanying report (Tech. Note GTD 85-4).

3.3 MULTI-MODULE GEOMETRY

If higher projectile speeds are desired, several alternatives are available. First, a hotter, lower molecular weight fluid can be used, increasing the sound speed of the fluid. Second, the nozzle can be redesigned to achieve a high Mach number $M = v_b/C_c$. Third, the distance between the capillary and the projectile can be reduced. The multi-module geometry is shown schematically in Figure 3.4. Its design takes advantage of all three cited methods of increasing the projectile velocity.

Figure 3.5 indicates the gas-dynamic processes which occur between electrical input and projectile acceleration. Properly

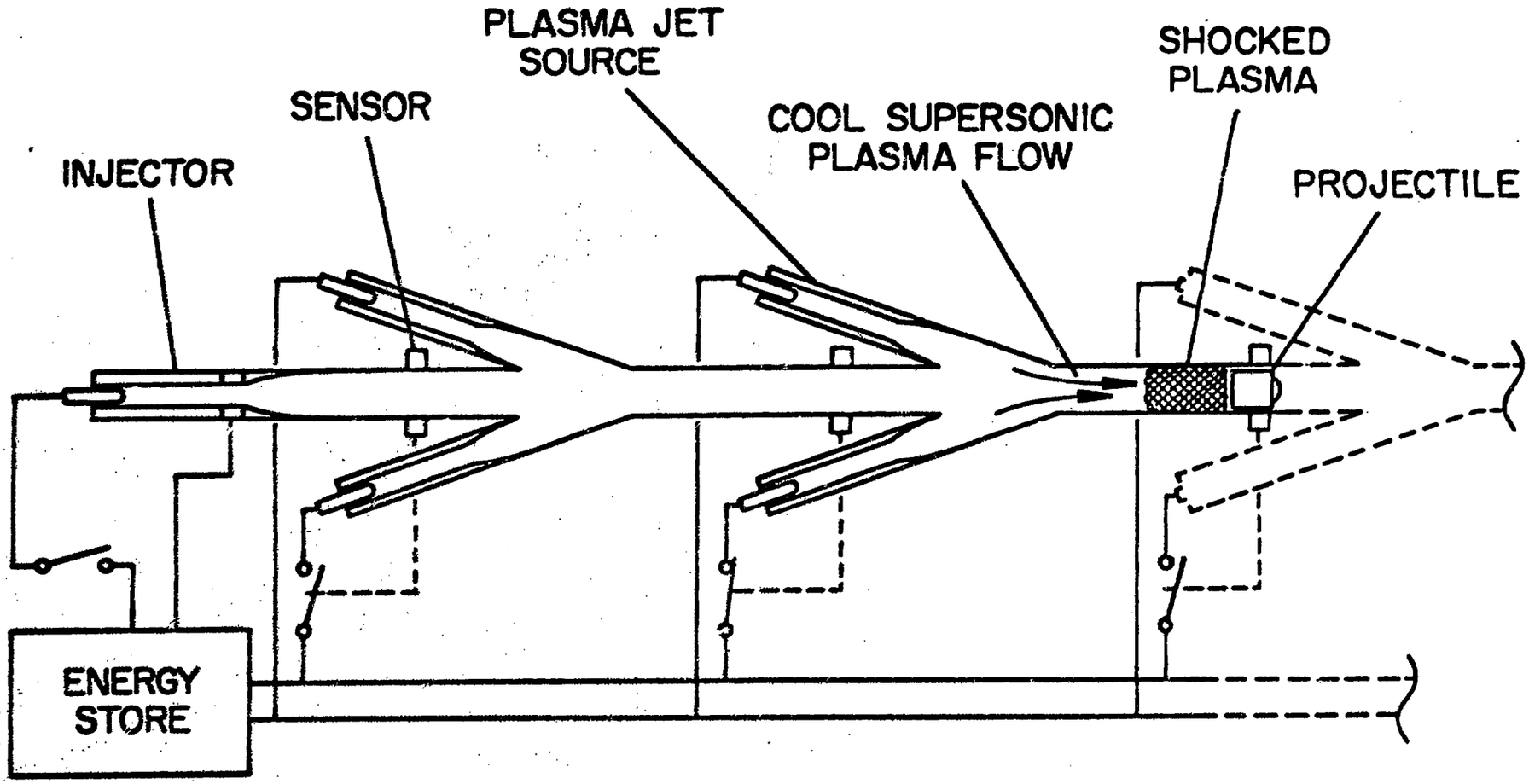

Figure 3.4

Schematic of a multi-module electrothermal accelerator. The first module performs like a conventional gun. Successive modules are switched on as the projectile passes.

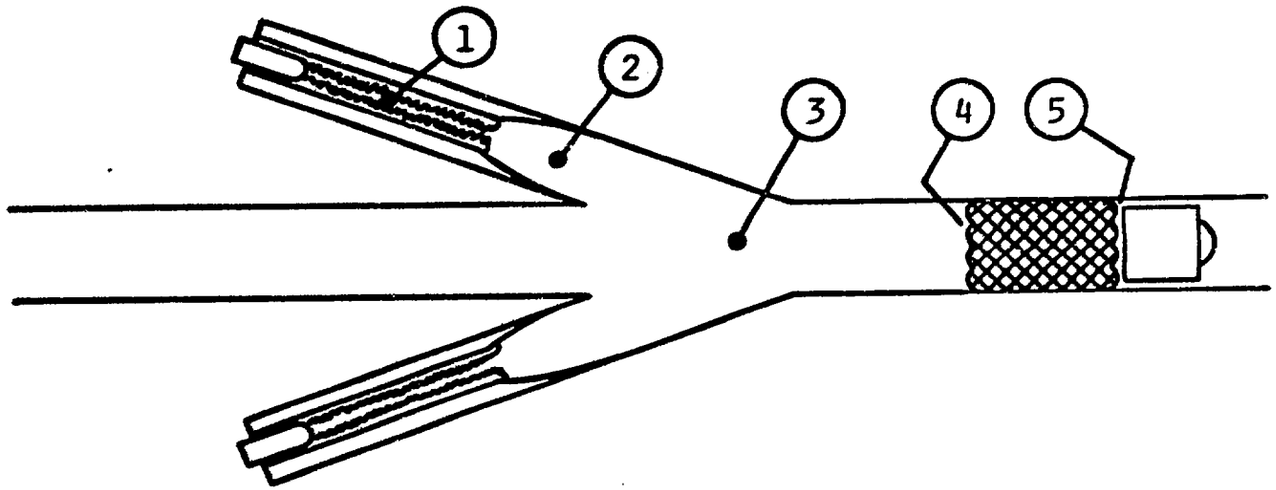

1 I^2R Heating of fluid

2 Supersonic Expansion in Nozzle

3 Pressure Drop at Bore Entrance

4 Shock Stagnation to Projectile Velocity

5 Gas Pressure Acceleration of Projectile

Figure 3.5

Details of the gas-dynamics in one module of a multi-module accelerator.

designed (see results below), these processes can produce efficient transfer of momentum,

$$M_u \delta U = \varepsilon \delta m_p (v_p - U) \quad , \tag{3.7}$$

from the plasma mass, δm_p, at velocity, v_p, to the projectile of mass M_u. The efficiency ε is a complicated function of the plasma parameters and projectile position and velocity.

4. COMPARISON WITH EXPERIMENT

The codes that have been developed during this contract have been continually compared with experiments. These comparisons have led both the changes in the design of experiments and improvements in the codes.

There are also some cases in which code results can be compared with analytic calculations. One of these concerns the ablation of material in a capillary.

4.1 DISCHARGE CHANNEL ABLATION

There is a limiting case in which the temperature of the plasma can be calculated inside the capillary. This is when the projectile is moving slowly and the heat loss to the wall is small compared to the input power. Then the energy input is balanced by the energy delivered to the wall by radiation.

$$2\pi r_c L_c P_{bb} = I^2 R \tag{4.1}$$

or

$$T = 2.2 \times 10^{-3} \left[\frac{I^2 Z \ln\Lambda}{r_c^3} \left(1 + \frac{2\nu_{eo}}{\nu_{ei}} \right) \right]^{\frac{2}{11}} \tag{4.2}$$

Typical values of the parameters are

$$I \sim 10^5 A$$
$$r_c \sim 2.2 \times 10^{-3} m \qquad (4.3)$$
$$L_c \sim 0.1 \text{ m}$$

so we expect temperatures of order

$$T \sim 4 \text{ eV} \qquad (4.4)$$

A few electron volts is typical, and the small exponent in Eq. 4.2 insures that the result is not sensitive to the parameters.

We can now estimate the mass flux, given an estimate of the terms in the denominator of Eq. 2.4. From the Sesame Equation of State tables, $H_s \sim 500$ MJ/Kg, for T = 4 eV and a density of 10^{27} m^{-3}, values which are typical of these capillary plasmas. These values yield a mass flux of

$$\frac{d\, m_{wall}}{dt} = \frac{\sigma_{bb} T^4 2\pi r_c L_c}{H_s} \sim 0.8 \text{ Kg/sec} \qquad (4.5)$$

or about

$$\delta m = \frac{d\, m_{wall}}{dt}\, \delta t \sim 8 \text{ mg} \qquad (4.6)$$

in 10 microseconds. In terms of the energy input, this means about 0.8 milligrams per KiloJoule. Now let us see how simulations compare with the analytic predictions.

Figure 4.1 illustrates the temperature obtained in a simulation of a capacitive discharge driving a capillary of the above dimensions. During the peak power input, the temperature briefly exceeds 5 eV, but 4 eV is a reasonable average value for around

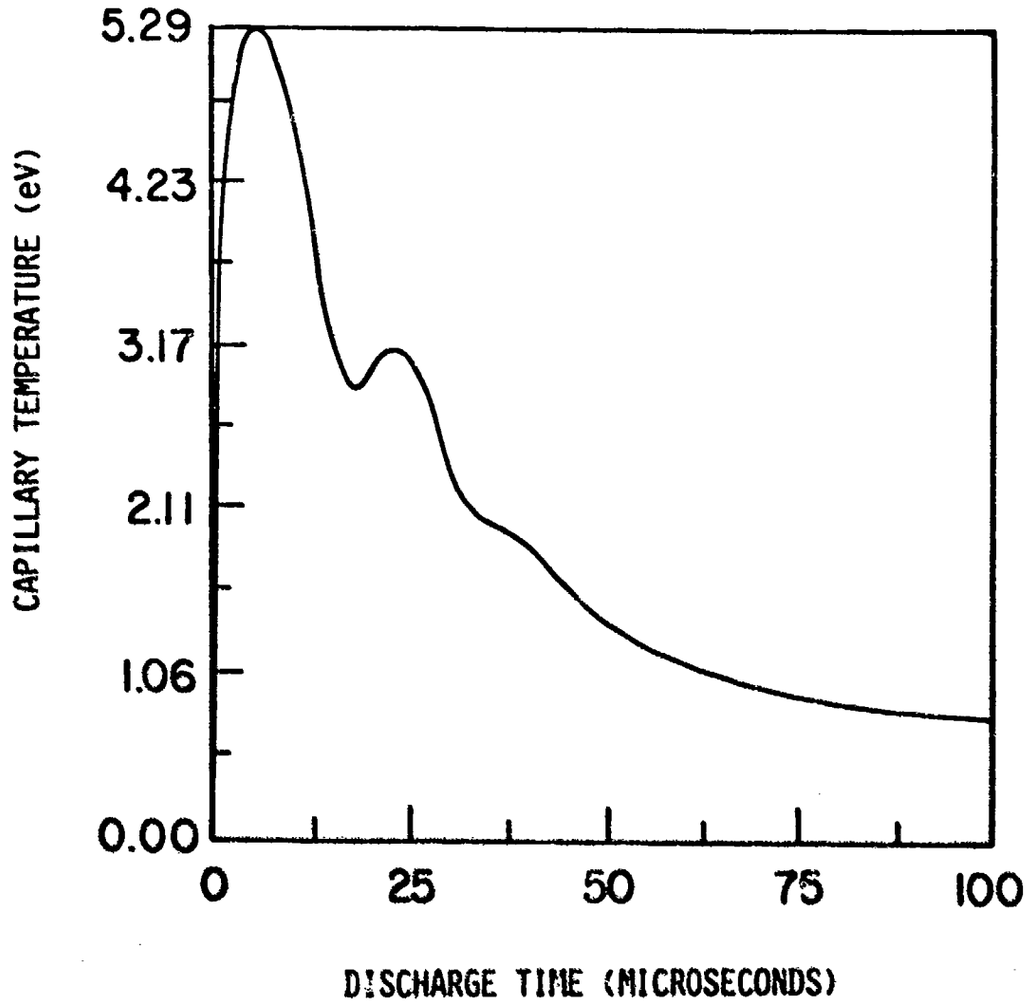

Figure 4.1

Temperature as a function of time in an RLC capillary discharge.

10 microseconds of high power input. The structure in the curve is due to the ringing of the discharge current. The temperature is what would be expected from the simple theory given above.

The ablated mass is shown in Figure 4.2. The solid line is the instantaneous ablation rate of material in the capillary. The broken line is the mass flux through the nozzle out of the capillary. The delay between the peaks of these two curves depends on the time it takes the gas to reach the nozzle. The dotted curve is the sound speed, which indicates both the characteristic speed of this exiting gas, and the factor by which the nozzle mass flux should be multiplied to determine the momentum produced by the capillary, and subsequently transported to the projectile. Note that 0.8 Kg/sec is a reasonable average value for the ablation rate, in agreement with the analytic prediction of Eq. 4.5. This provides an analytic benchmark for the ablation rate in the capillary.

Next, a computer model can integrate the instantaneous mass flux over a complete discharge cycle and determine the total ablated mass for an experiment. This has been done for a series of experiments in which different total energies were deposited in the cartridge during each experiment. The results are presented in Figure 4.3. This shows the experimental data, and simulations using the same experimental parameters. The error bars on the experimental data are large, because the mass loss is a difficult measurement. However, the difference between experiment and theory is large enough to suggest that it is real. This probably means that material is removed by advection and heat conduction, in addition to the radiation that was included in these calculations. When we incorporate our recently-developed turbulent heat transport model (TN GTD 85-4) in the computer codes, we expect this agreement to improve.

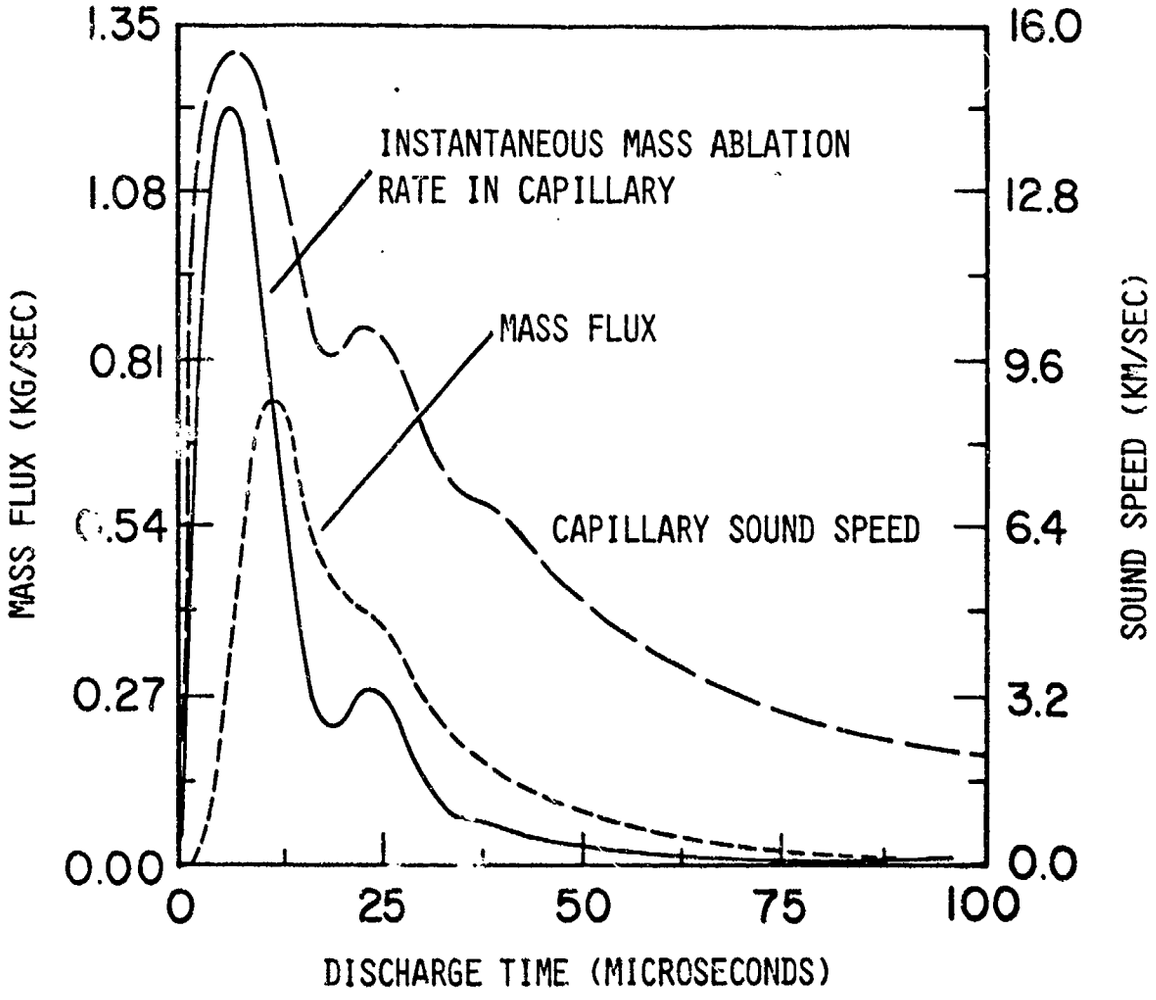

Figure 4.2

Mass ablation and transport versus time in a capillary discharge.

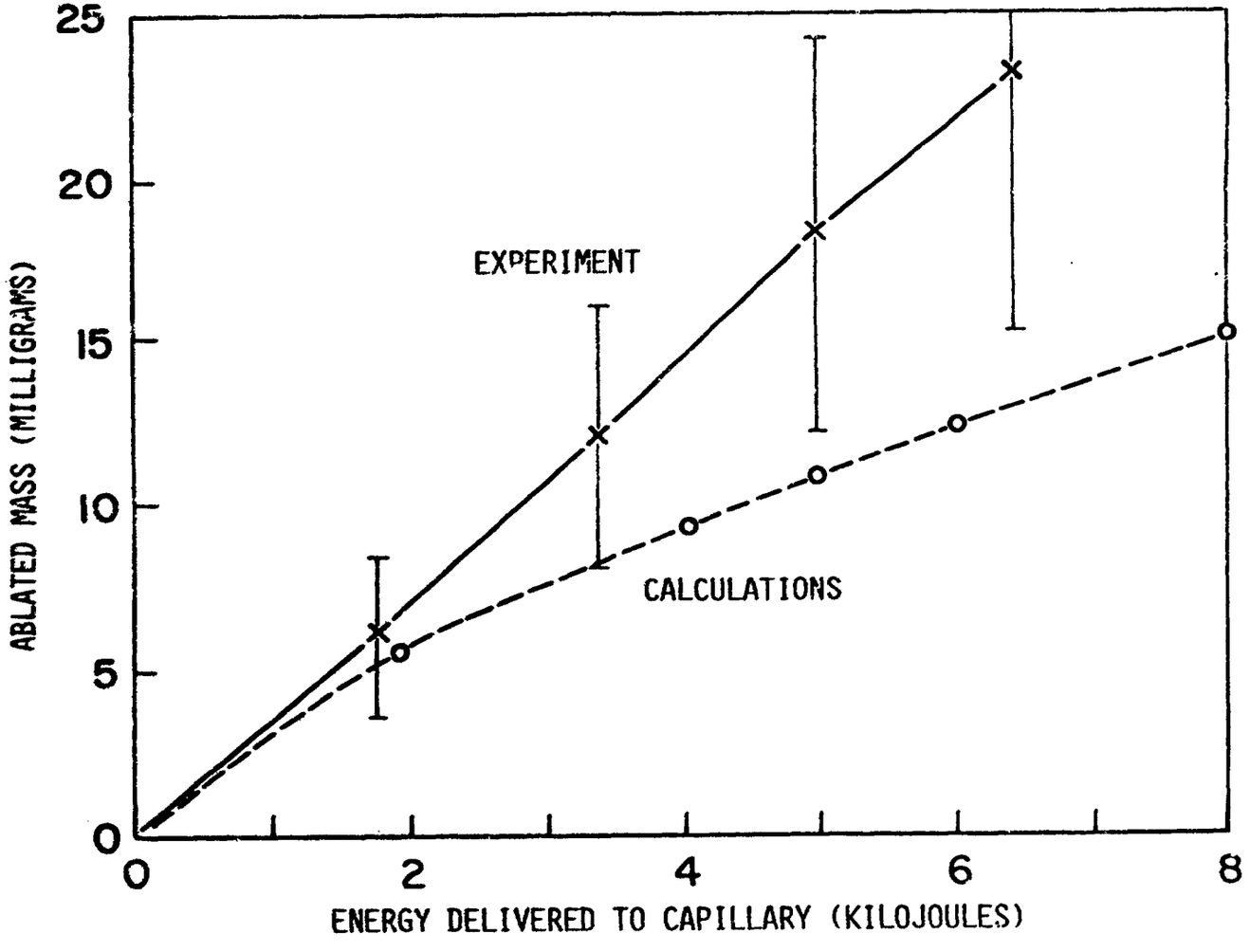

Figure 4.3

Capillary ablation versus discharge energy for a series of experiments

4.2 PLASMA PRESSURE

An electrothermal gun is an energy conversion system. First, it converts electical energy into plasma internal and kinetic energy. Then the plasma performs work on the projectile and converts much of its energy into projectile kinetic energy. The plasma pressure is a key figure of merit for the second conversion.

If the material limits did not matter, the ideal operation of an ET gun (and a conventional gun for that matter) would involve delivering the available energy to the propelling fluid as quickly as possible, making the pressure as high as possible, and thus accelerating the projectile to the desired speed in a very short distance, before it has traveled far down the barrel. This is the description of a bomb, not a gun.

The material strengths of the barrel and other components limit the maximum pressure which can be contained in a particular gun design. This suggests a more realistic "ideal design" for a gun. The pressure should rapidly rise to some selected value, and then that value should be maintained until the available energy is expended.

Conventional chemical propellant guns cannot do this, because the rate of chemical energy release cannot be controlled in the required matter. However, the electrical power supply of an ET gun can be programmed to accomplish just such a feat.

Computer simulations of experiments show the relationship between the power input and resulting pressure. Thus computer "experiments" can be performed to determine what power input will produce a flat pressure profile. Maid 8 has been used to perform these calculations.

Given the required power profile and the capillary resistance profile, a power supply can be designed to deliver it. This was done using PCAP.

Figure 4.4 shows the experimental power input to an experiment, the computed average pressure, <P>, and the pressure on the base of the projectile, P_b. The objective of the experiment was to keep the pressure below 5 kBars (5×10^8 Pascals, or 74,000 psi), while maintaining as much pressure on the projectile as possible. According to the simulation, it has accomplished that objective, by quickly bringing the pressure up to 4.5 kBar, and then remaining near that pressure until the available energy is consumed.

The computer code predicts the internal pressure in Figure 4.4. It remains to verify that this prediction is correct, since much of the dynamics depends on this pressure.

The experiment was instrumented with a pressure probe in the wall of the gun tube. Figure 4.5 compares the signal from this experimental probe with the pressure at the probe location, 18.5 cm from the starting-point of the projectile.

The simulation pressure and experimental data both show a steep rise at 600 microseconds. That is, they agree on the arrival time of the projectile at the location of the pressure probe. They also are in excellent agreement on the pressure after 1000 microseconds, showing that the code accurately models the fluid flow down the barrel once the flow is established.

The source of the disagreement between 700 and 900 microseconds is unclear. It is possible that turbulence, liquid water or other debris following behind the projectile, or other dynamical effects, are causing a reduction in pressure just behind the projectile. It is also possible that the shocks delivered to the gun tube by the arrival of the projectile and the high pressure

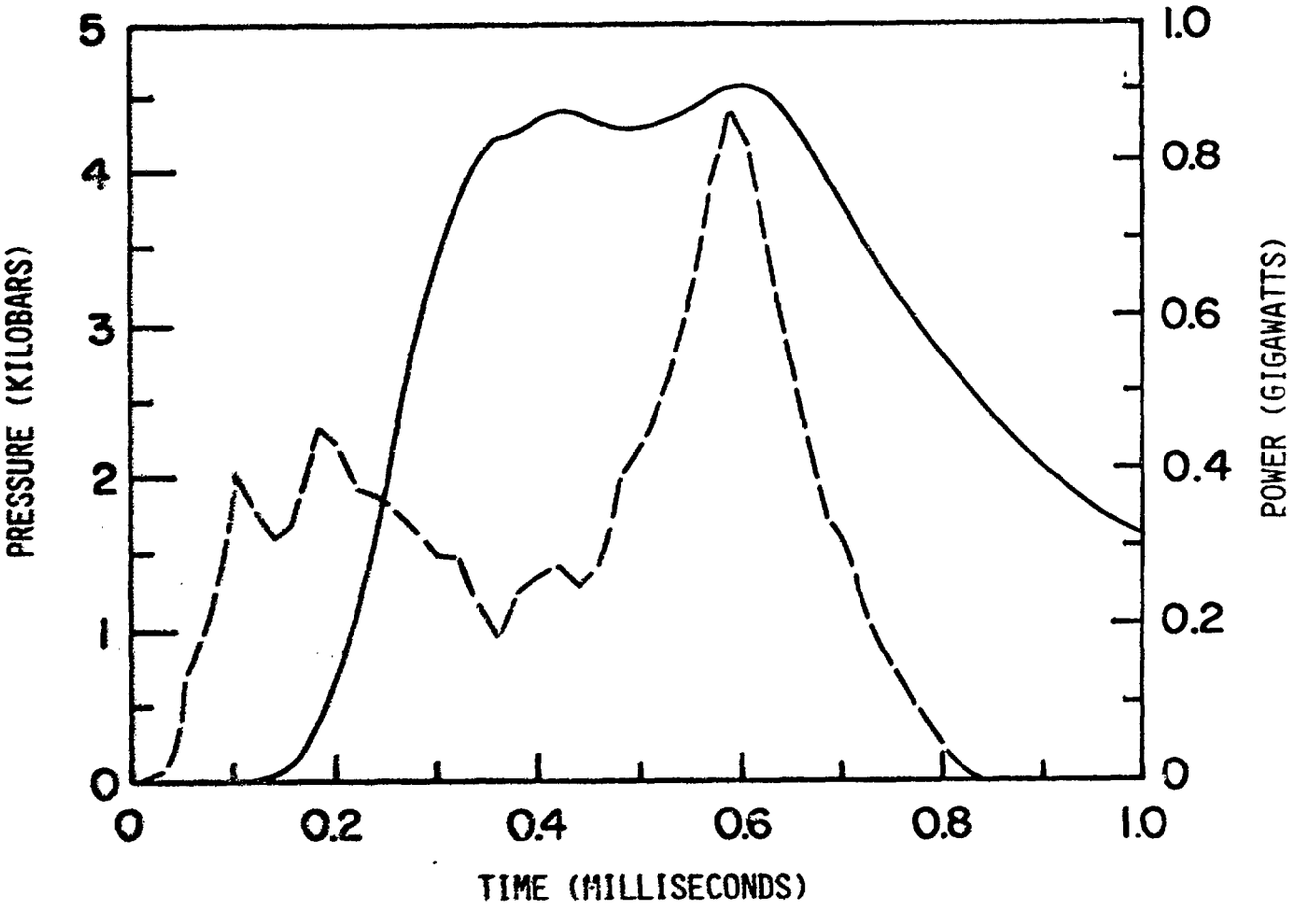

Figure 4.4

Shot C075 electrical power input (dashed) and average pressure during the discharge. Note the nearly constant pressure profile.

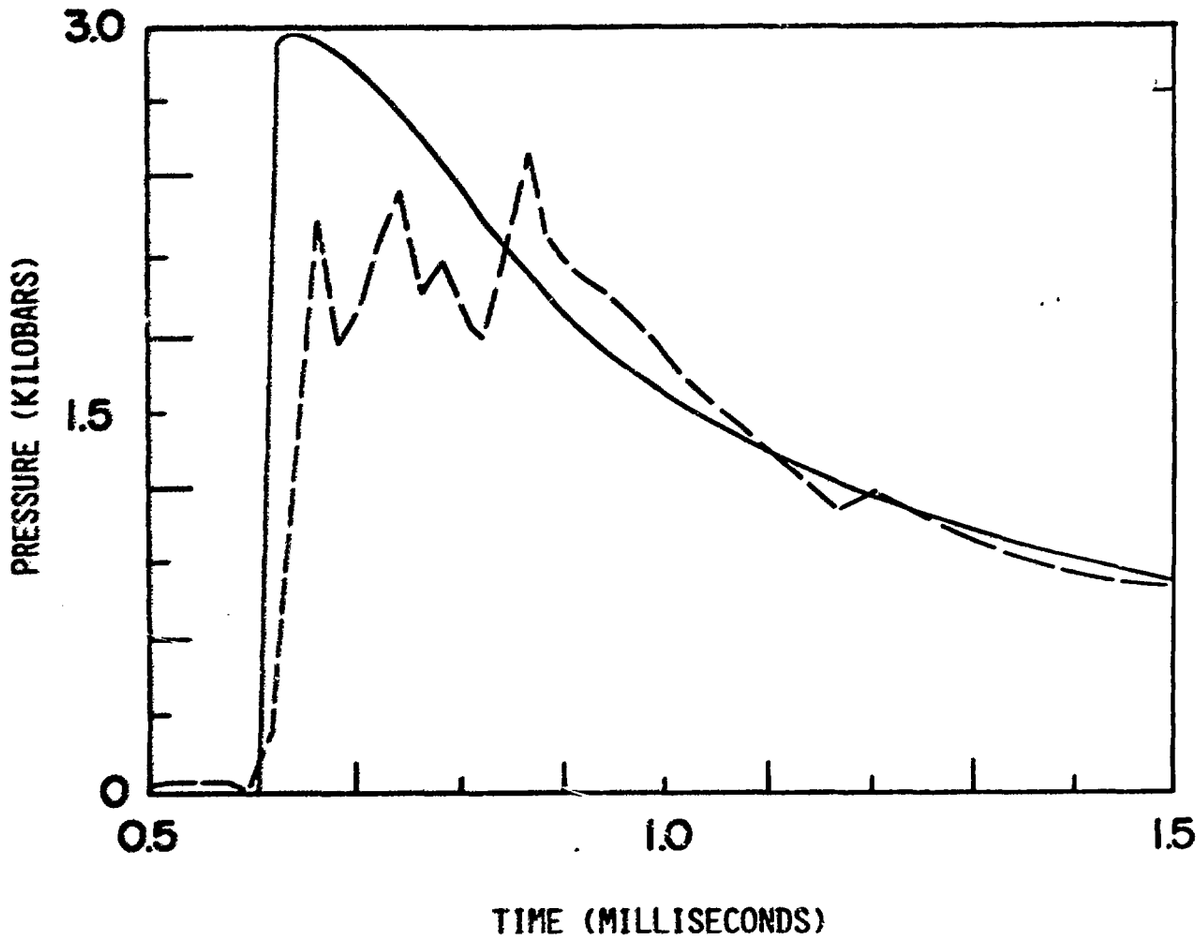

Figure 4.5

Shot C075 pressure probe data (dashed) and calculated (simulation) pressure at probe location. Note displaced origin of time.

fluid disturb the pressure probe, and it requires several hundred microseconds for this disturbance to relax.

It is important to establish the true cause of this discrepancy between 700 and 900 microseconds, because the pressure immediately behind the projectile provides the propelling force. After all, high projectile velocity is the ultimate achievement of a projectile launcher.

4.3 PROJECTILE VELOCITY

The pressure which acts on the projectile accelerates it down the gun barrel. As the projectile gets further from the source of the propelling fluid, the ratio of the projectile pressure to the capillary pressure, P_b/P_c, drops according to Eq. 3.6.

For the experiment described in the previous section that model is optimistic. Figure 4.6 shows the projectile speed, as predicted by the code, and the average pressure <P> and projectile base pressure, P_b. The "x" corresponds to the experimental projectile velocity, about 350 m/sec (or 20%) below the prediction. Recall however that Figure 4.5 showed the experiment and code gave the same arrival time for the projectile at the probe postion, and therefore the same average velocity up to that point. This shows that the MAID 8 code is not correctly calculating the dynamics as the projectile moves further down the barrel.

Figure 4.7 shows one factor which may be involved. The projectile speed, V_b, is plotted along with the average sound speed. The code predicts that the projectile travels

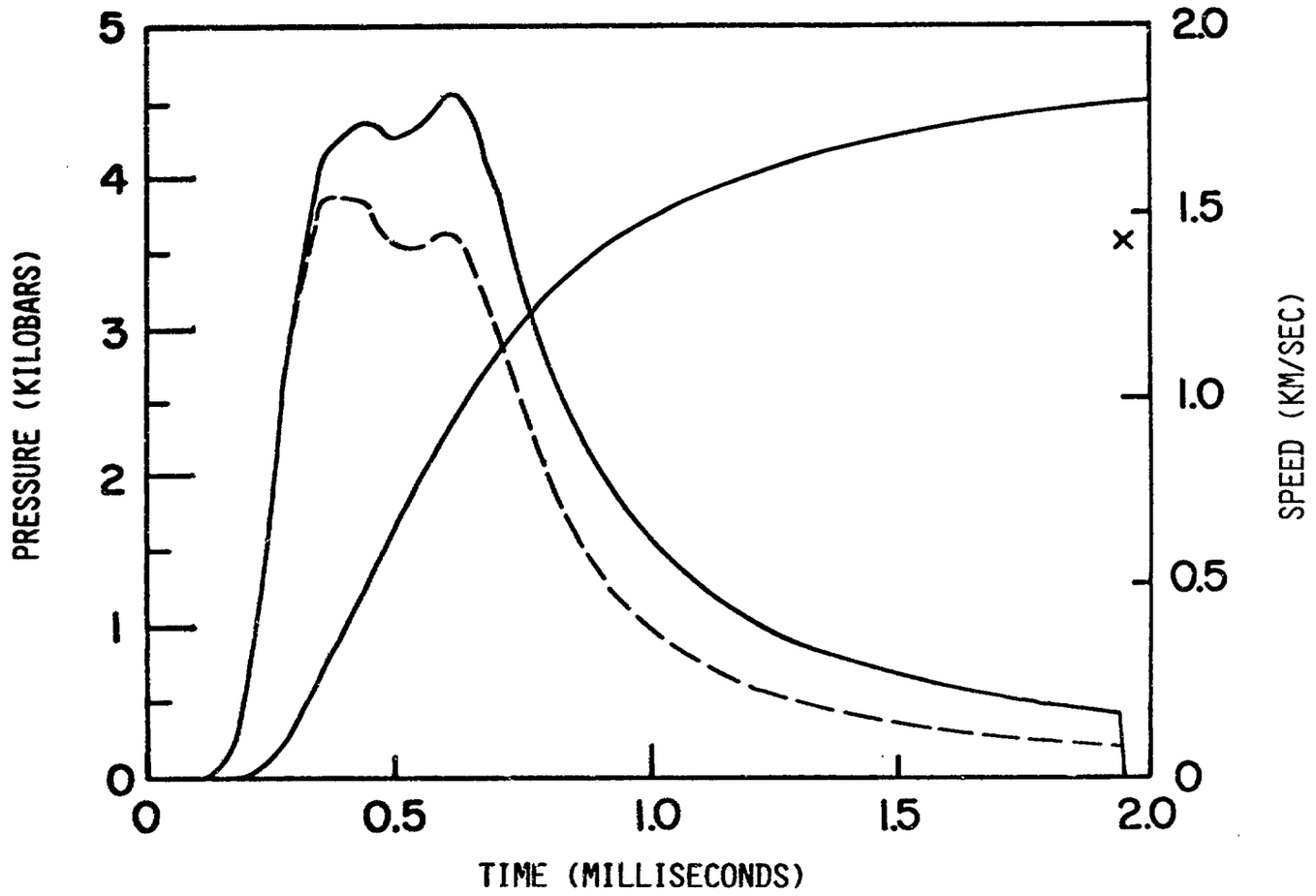

Figure 4.6

Shot C075 average pressure, projectile base pressure (dashed) and projectile speed (rising). The experimental muzzle velocity is given by the "x".

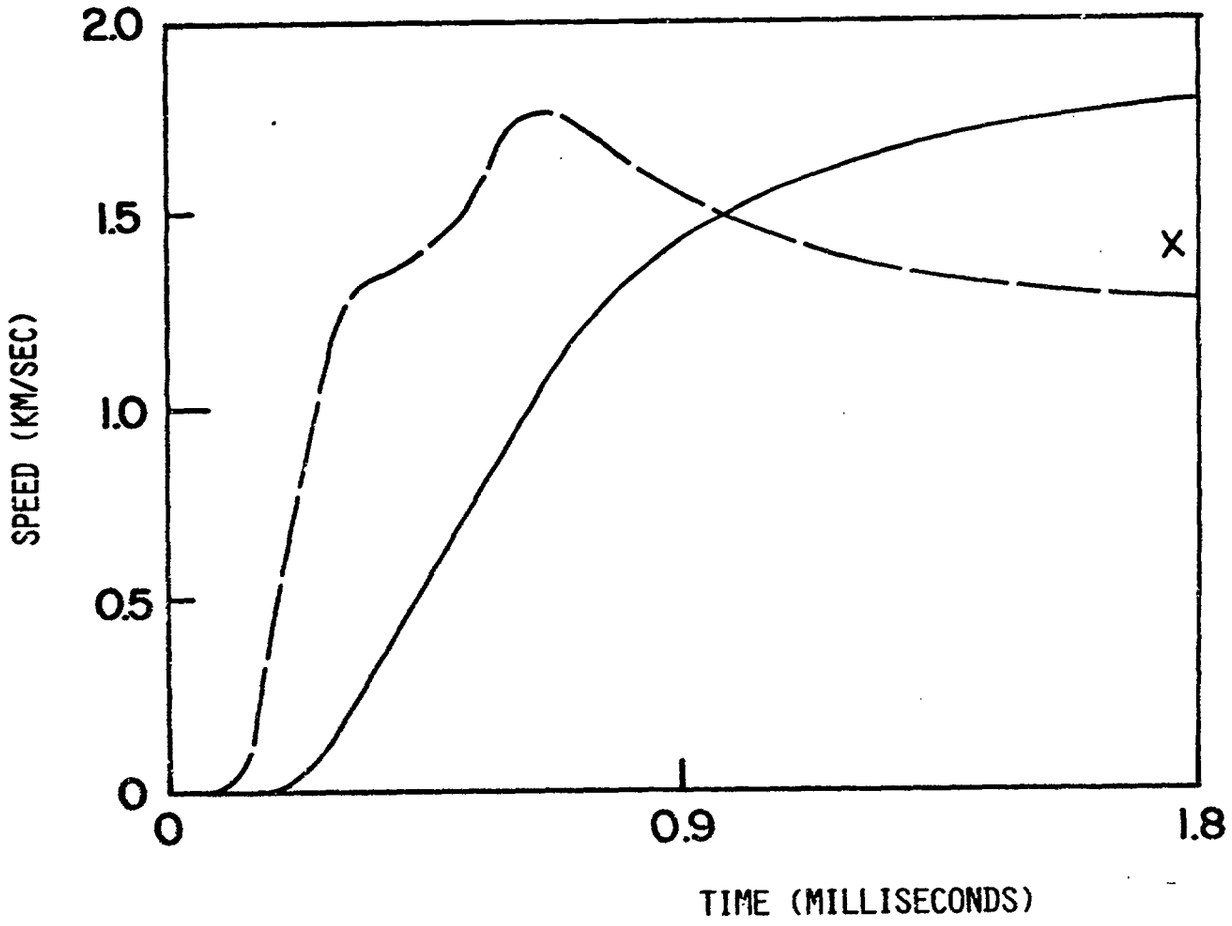

Figure 4.7

Shot C075 projectile speed and average sound speed (dashed). The "x" is the experimental muzzle velocity.

considerably faster than the sound speed. Theoretical analysis of turbulent flow down tubes suggests that this may be very difficult to achieve (TM GTD 85-4).

The next three figures provide a contrasting case, in which the experiment and code prediction of the velocity agree. Figure 4.8 shows <P>, P_b and V_b for an earlier experiment in which we had not yet achieved constant pressure. Note the close agreement between the predicted velocity and experiment.

Figures 4.9 and 4.10 correspond to Figures 4.4 and 4.7, to provide a complete comparison between these two cases. Note in Figure 4.10 that the sound speed exceeds the projectile speed throughout the experiment.

In conclusion, the MAID 8 code appears to accurately model the experiments when the plasma sound speed exceeds the muzzle velocity. When this is not the case, the code overestimates the projectile speed. This can probably be corrected by incorporating the recently-developed theoretical models of turbulent pipe flow into the code.

5. PERFORMANCE PREDICTIONS

In the preceding section we saw examples of code predictions that could be directly compared with experiment. These included ablation rates, projectile velocity and various internal pressures. We also encountered quantities which are not easy to measure directly, such as the fluid sound speed, C_c, and the adiabatic function, γ. The present chapter concentrates on quantities which are not easily measured. The objective is to identify parameters which may improve the performance of the gun system.

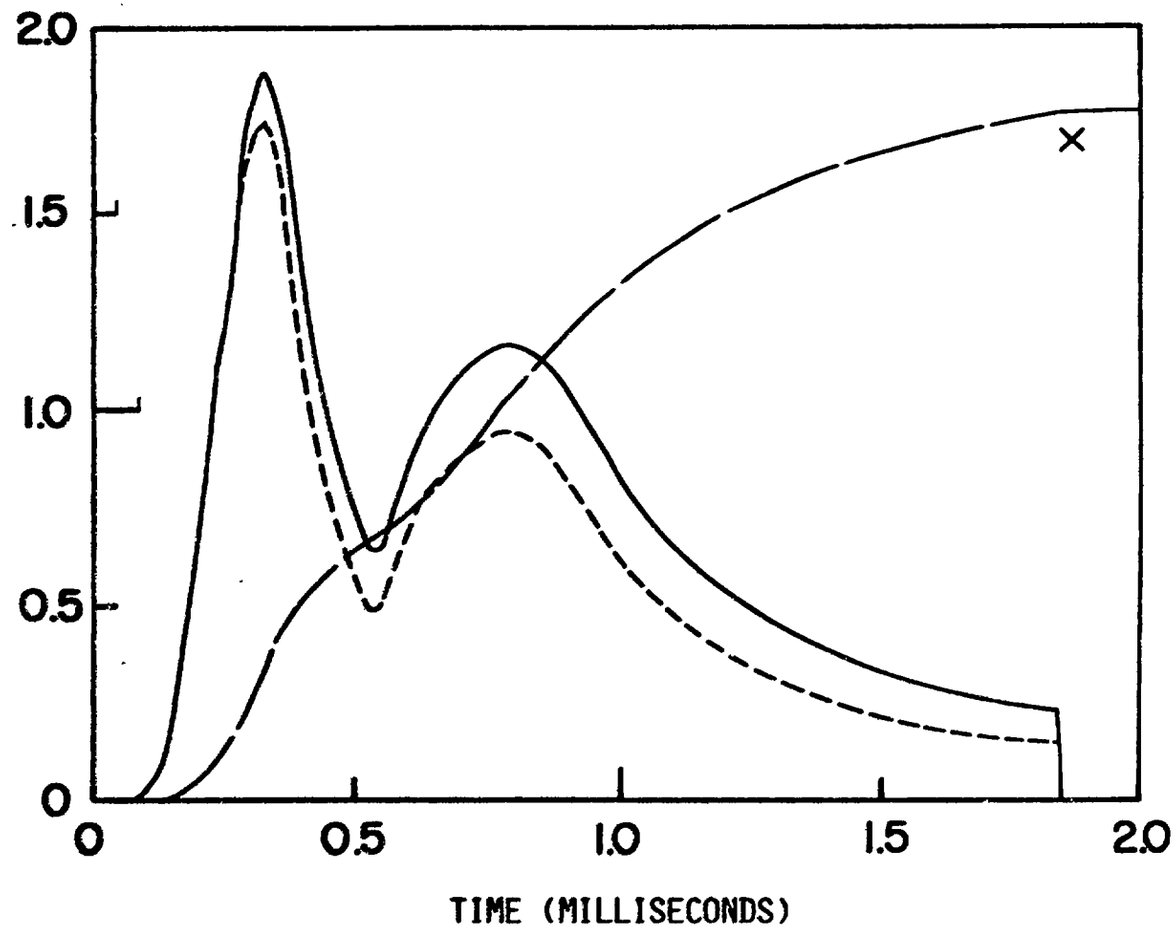

Figure 4.8

Shot C029 average pressure, projectile base pressure (dashed) and projectile speed (rising). Compare Figure 4.6, which shows a later, constant-pressure shot.

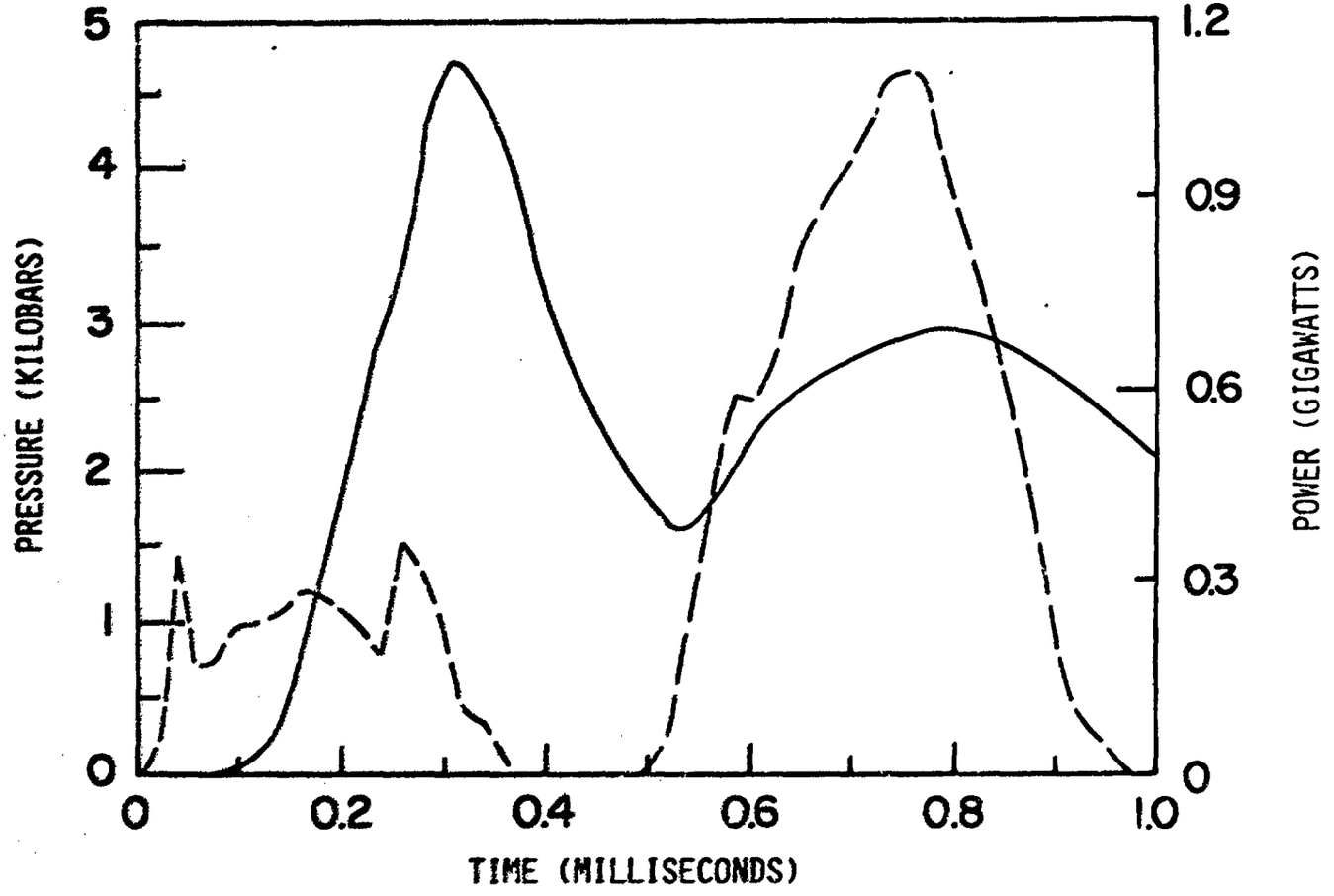

Figure 4.9

Shot C029 electrical power input (dashed) and average pressure. Compare Figure 4.4.

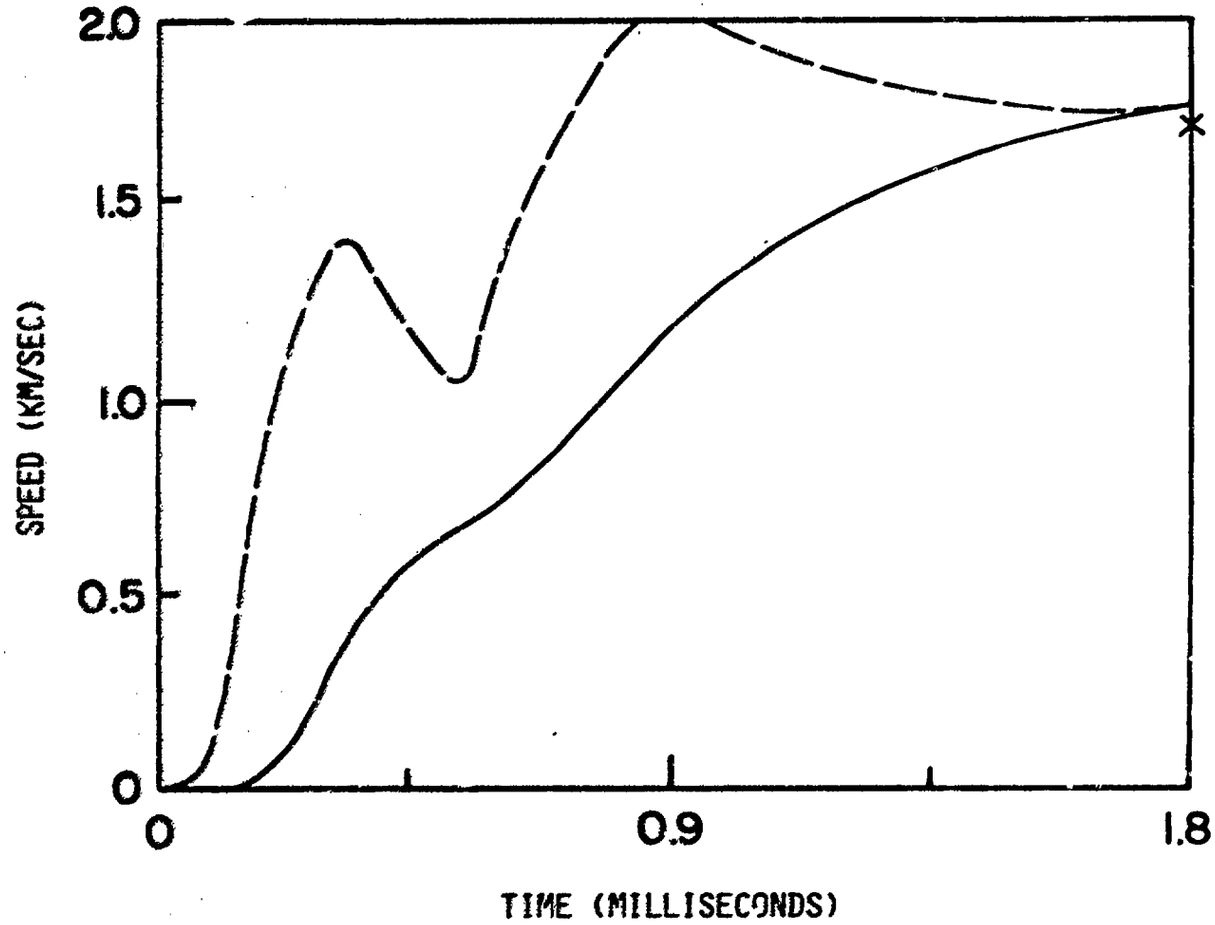

Figure 4.10

Shot C029 projectile speed and average sound speed (dashed). Compare Figure 4.7.

5.1 INTERNAL PLASMA DYNAMICS

The performance of electrothermal gun systems depends on many factors. While the electrical circuit properties can be controlled externally, the internal fluid properties are less easily controlled. Over the course of this contract, we have greatly improved the computer model of the plasma properties.

The MAID series of codes now use the full SESAME formulation of the material equation-of-state which has been developed by Los Alamos National Laboratory, (LASL). The subroutines provided by LASL have been extended to provide additional information about the driving fluid, such as the degree of ionization and the adiabatic parameter defined by Equation 2.5.

The data available through SESAME shows that the choice of material can have a dramatic effect on the plasma behavior, and thus on the internal dynamics of the gun. To illustrate this, consider two candidate materials. One is polyethelene, $(CH_2)_n$, one of the initial choices as an ablatable material. Second, consider pure hydrogen, H_2, which represents 67% of the atoms in polyethelene.

Figure 5.1 shows the temperature dependence of the Gruneisen coefficient

$$G = P/W = \gamma - 1$$

The solid curve is for hydrogen and the broken curve is for polyethelene. The importance of G is that it measures the fraction of the energy deposited in the fluid which is available as pressure, to accelerate the projectile. A larger G means a higher projectile acceleration for a given energy input.

Figure 5.2 presents the sound speed versus temperature for the same parameters. It is apparent that the choice of material has a dramatic effect on the properties of the fluid.

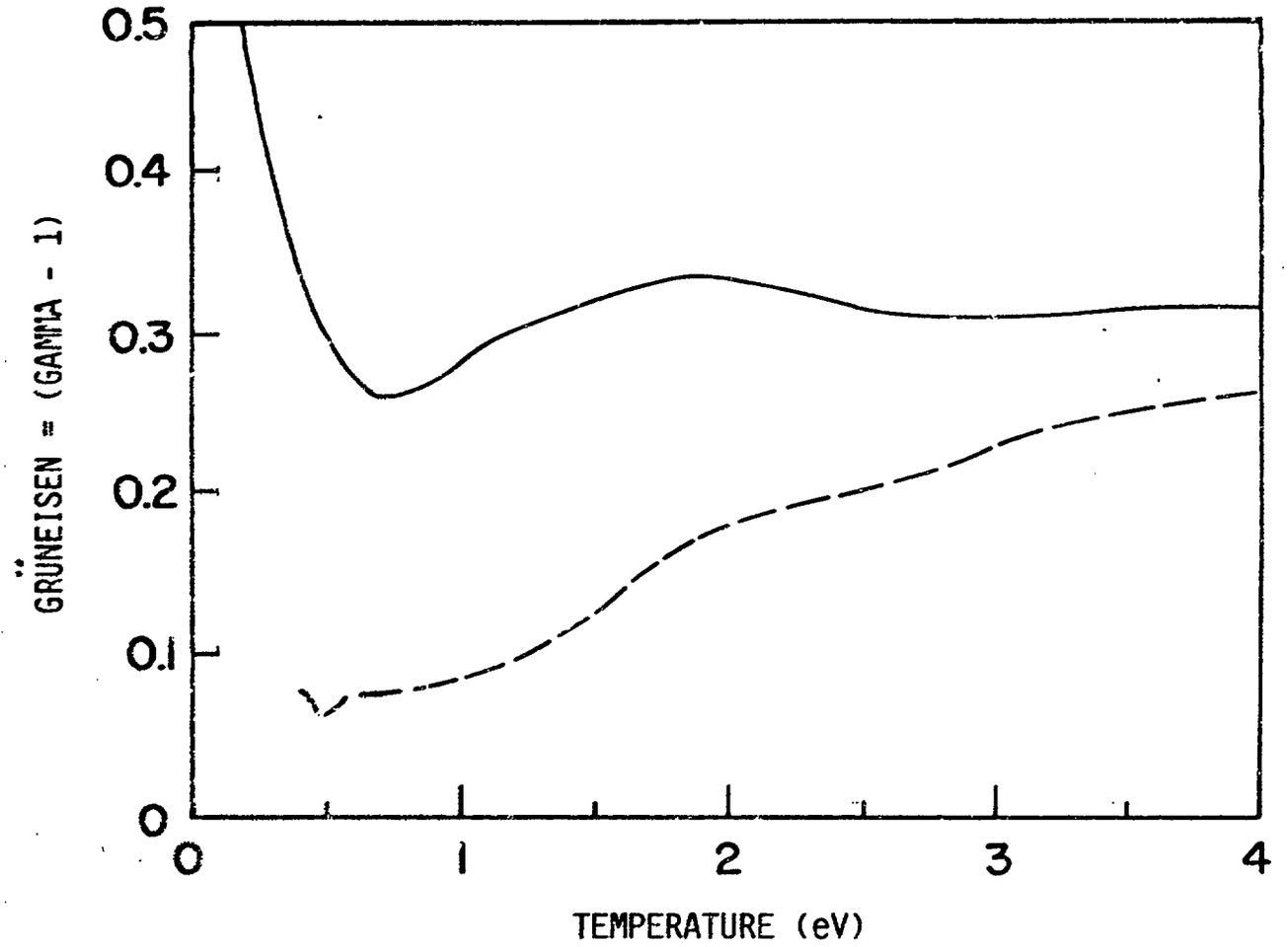

Figure 5.1

Grüneisen coefficeint versus temperature for polyethlene (broken) and hydrogen at 5 kilobars. The temperature is in electron volts, where 1 eV = 11,600 degrees Kelvin.

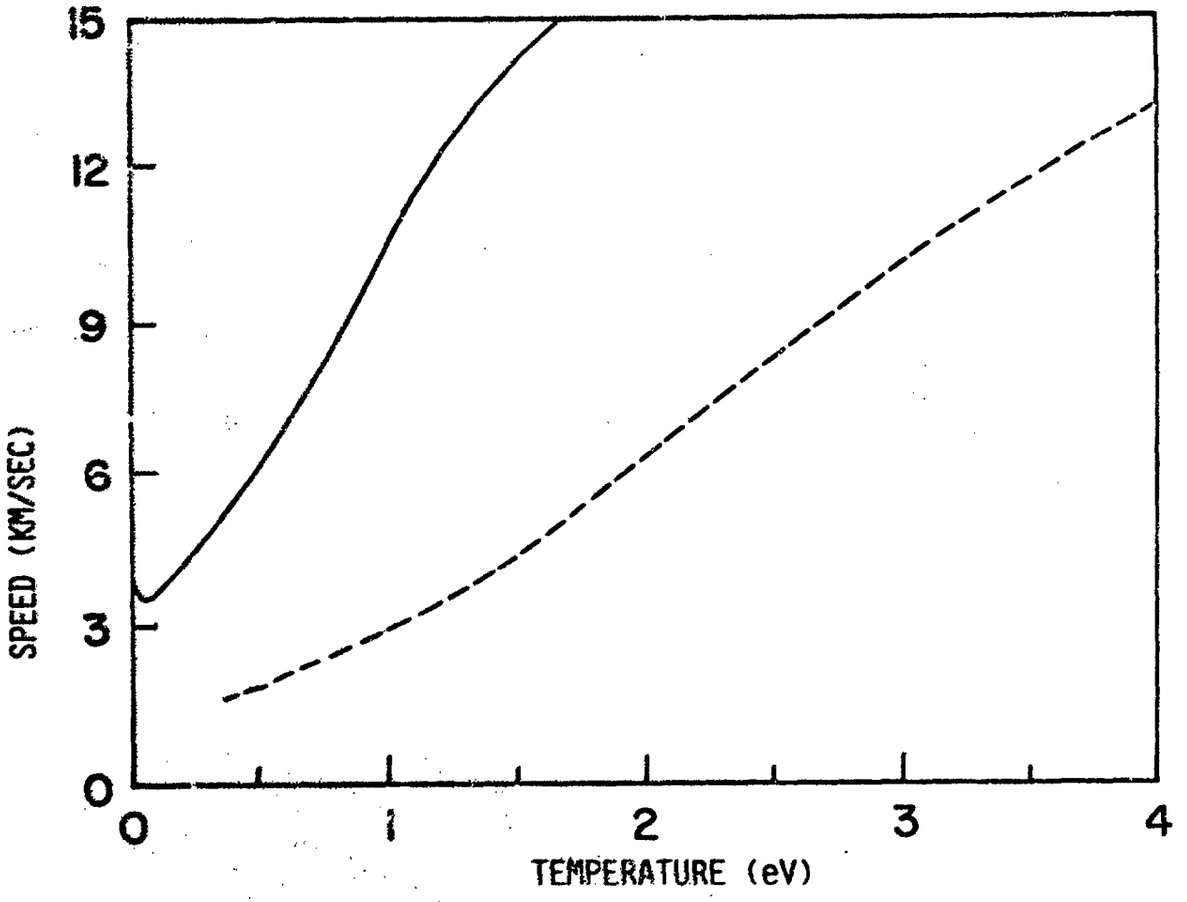

Figure 5.2

Sound speed versus temperature for polyethylene (broken) and hydrogen at 5 kilobars.

As we saw in the preceding section, properties such as the sound speed strongly influence the ability of the fluid to accelerate the projectile far down the barrel. Therefore these differences in the fluid properties are of great practical importance. Various materials, including pentane, methanol and lithium hydride have been considered as candidates for propellant fluid. Because of the different material properties, it is usually necessary to change the power input as well as the fluid. The merits of the various choices are presently being analyzed.

5.2 EFFICIENCY PREDICTIONS

The efficiency of the system is a straightforward and very important measurement for single-stage gun systems. We have found that for many experiments, code predictions of efficiency agree well with the experimental results when the code accurately predicts the muzzle velocity.

When additional acceleration modules are added, the comparison becomes much more difficult, because many new variables are present, so it is much harder to perform a code calculation which accurately models all the conditions which were present in the experiment.

For these more complicated systems, one valuable contribution of calculations is to predict the performance available from a module as a function of the internal parameters. Such calculations show what performance is possible, and how the internal parameters should be adjusted to achieve it.

Figure 3.4 shows the full complexity of the geometry of an acceleration module. The KInetic Weapon Impulse, (KIWI) code has been developed to model the fluid flow in this geometry. It uses a simplified equation-of-state for the fluid, but models the full dynamics of the capillary interior, nozzle expansion, flow down the barrel, and the interaction of the fluid with the projectile.

These studies have shown that electrothermal modules are capable of efficiencies over 60% for hydrogen. The challange is then to define the conditions under which such efficiencies can be achieved in the laboratory.

Figure 5.3 shows the KIWI prediction of module efficiency with two key ratios as independent parameters. One is the Mach number, M, defined in Eq. 3.4. This is determined by the nozzle geometry and the temperature and equation of state of the fluid.

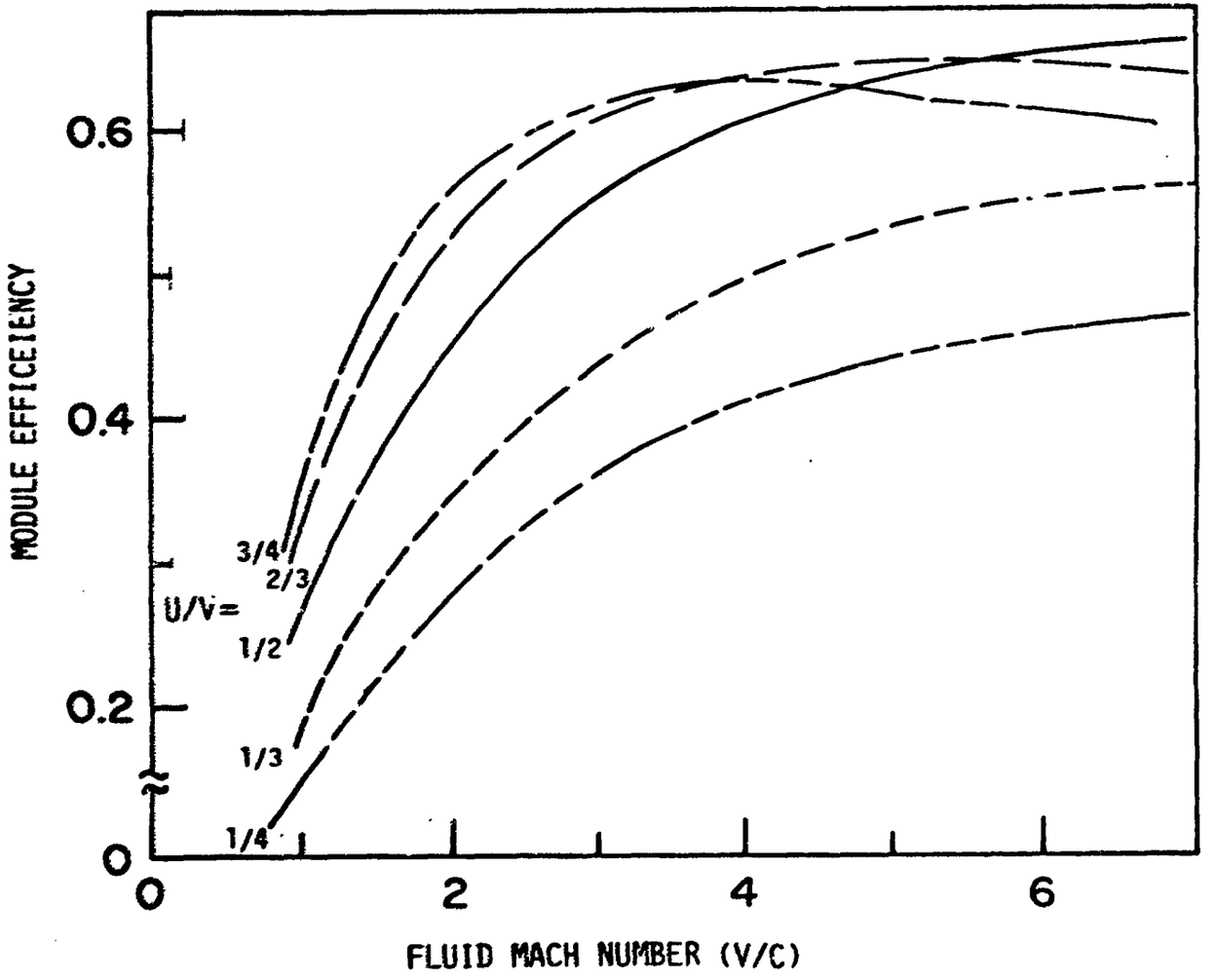

Figure 5.3

Efficiency (projectile energy increase divided by electrical energy input) versus Mach number, M (fluid flow speed divided by sound speed), for several ratios of projectile speed (U) over fluid flow speed (V).

The other parameter is the ratio of the projectile velocity to the flow velocity, U/v_b.

It is clear from Figure 5.3 that modest Mach numbers, $2<M<4$, and flow speeds somewhat greater than the projectile speed, $4v_b/3 < U < 3v_b/2$, produce optimum performance.

5.3 ADVANCED SYSTEMS

The ultimate demonstration of code predictions is the design of future experiments, when the codes are used to describe a system which differs substantially from present-day experiments. Various pratical constraints are applied, and overall system performance is predicted. Maid 8 and KIWI calculations were combined to design a launcher for projectiles with masses of several kilograms to velocities over 12 km/sec. The power supply is assumed to be limited to an output of 5 gigawatts.

Figure 5.4 shows the power input plus average and projectile base pressures, as in Figures 4.4 and 4.6. Here the power input has been tailored to hold the projectile base pressure constant until the power reaches 5 GW, and then it maintains that power until the available energy is consumed.

Following the initial gun-like stage, the projectile is driven by a series of modules, configured to produce uniform acceleration. Depending on the material properties of the propelling fluid and barrel liner, each can accelerate the projectile for a given period of time, typically 200 microseconds, after which the propelling fluid is removed in preparation for the next module.

Figure 5.5 shows the velocity versus time as predicted by the codes. According to the KIWI model, the modules are capable of much higher final velocities; this calculation simply

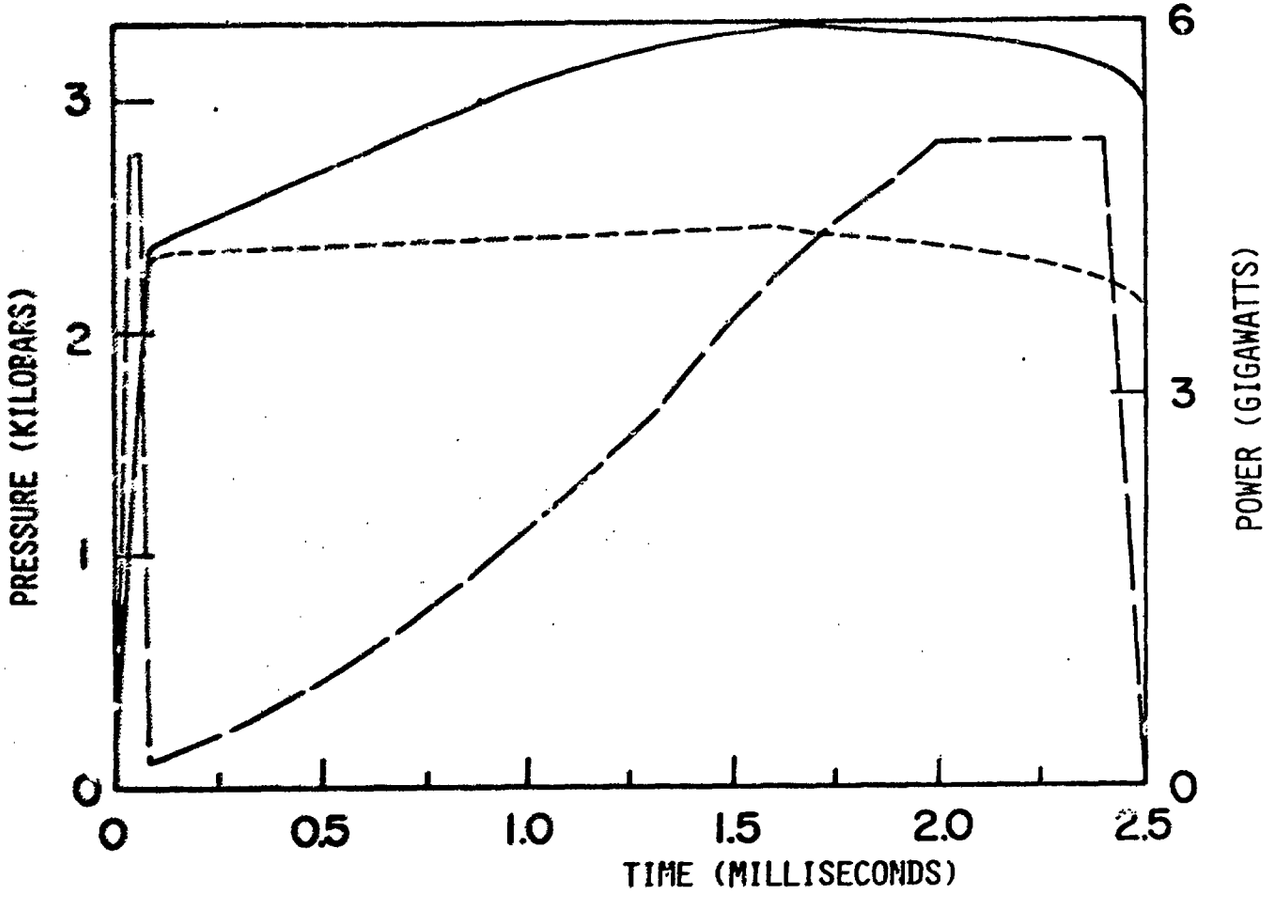

Figure 5.4

Advanced system first stage electical power input (broken), average pressure (higher solid) and projectile base pressure (dashed) versus time. The power input is limited to 5 GW.

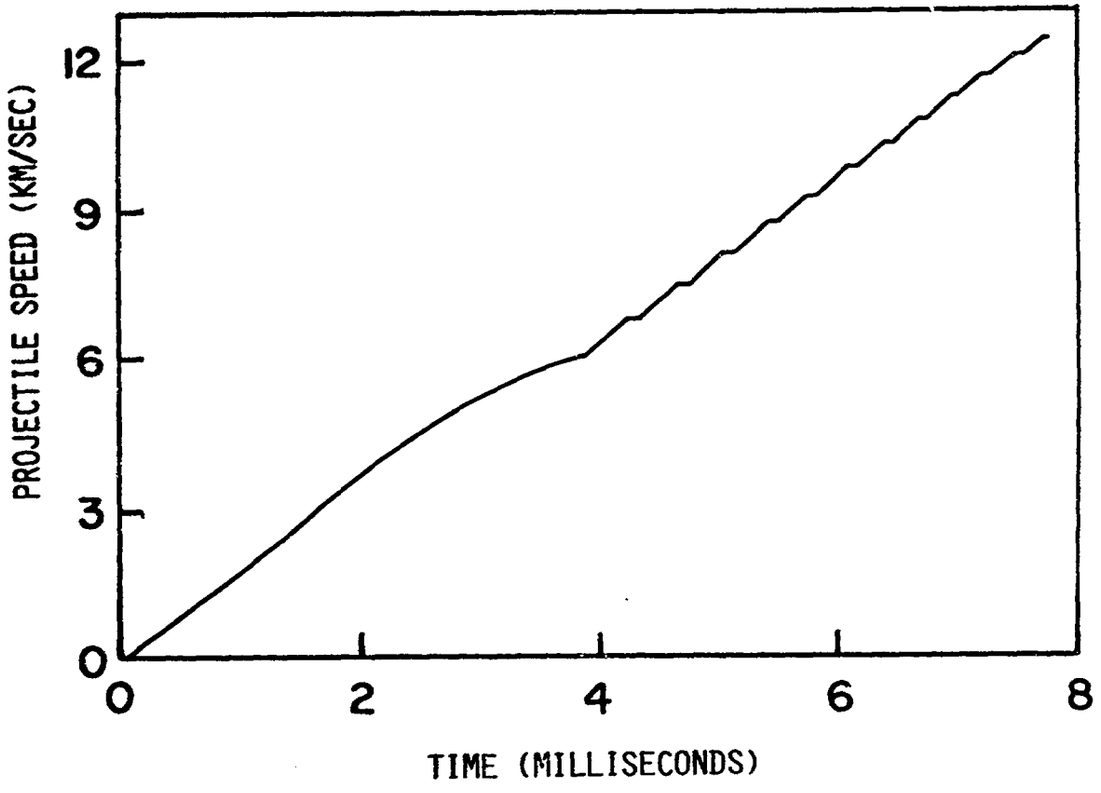

Figure 5.5

Advanced system projectile velocity versus time in a multi-module accelerator.

illustrates the operation up to 12 km/sec, or about "escape velocity" from the surface of the earth.

6. SUMMARY

The MAID and KIWI codes have been developed and applied to the study of electrothermal mass accelerators. They have been benchmarked against experiment, and show good agreement with it. They have been used to predict the performance of devices presently being designed.

These codes incorporate detailed models of the external driving electric circuit and the basic physics processes by which joule heating generates plasma from ablating materials in the capillary discharge. They have been extended to multi-dimensional flows of multi-species plasmas in relatively complex geometries.

The ablation and survival of capillary walls has been examined (Section 4.1), along with the effect of repeated discharges (Sections 4.2 and 5.1) and the impact of high-pressure plasma on the projetile (Sections 4.3 and 5.1). Calculations have been compared with experiments, and produce excellent agreement for projectile arrival time and pressure during fully developed flow (Figure 4.5) and muzzle velocity (Figure 4.8). Results of cartridge ablation studies show that experimental ablation rates are somewhat higher than predicted (Figure 4.3), but some known flow erosion phenomena have not yet been included in the models.

The SESAME chemistry package has been incorporated in the code, and has been used to investigate the influence of different materials (Figures 5.1 and 5.2) on the performance of accelerators. As an illustration, for a fixed temperature, hydrogen has a much higher sound speed than polyethylene (Figure 5.2), so it is

capable of reaching higher muzzle velocities for the same temperature and gun geometry.

More complex gun cavity geometries have been examined (Figure 3.2) and the results of simulation (Figures 4.6 and 4.7) show that the geometry affects the fluid flow more than the present model anticipates.

The MAID codes have been extended to simulate multi-module accelerators. The KIWI code extends this capability further. The inclusion of drift sections between modules has made possible the elimination of interference between successive modules, without significantly reducing acceleration rates. (The effect of the drift spaces is to introduce the horizontal segments in the acceleration profile, Figure 5.5.)

The analysis of the ablation rate and heat transport into the walls of the capillary and barrel walls has made possible the analysis of the lifetime and rep-rate capability of electrothermal launchers. The inclusion of powder fill in the capillaries and a fluid mixing chamber in front of the capillary (Figure 3.3) has extended the lifetime of the barrel essentially indefinitely. In the laboratory, conventional gun barrels have now been used for more than 100 electrothermal shots. Using a design in which the capillary and mixing chamber are included with the projectile in a replaceable cartridge, the rep-ratability of the system seems to be limited only by the rate at which the cartridge can be removed and replaced, by a mechanism similar to the auto-loader in a conventional gun.